Oceanologia, 67 (2)/2025, 67207
Polish Academy of Sciences
Institute of Oceanology

https://doi.org/10.5697/QPUN2882

Analyzing Ogurja Island's shoreline changes in response to the Caspian Sea water level decline

Rahimeh Shamsaie[1], Danial Ghaderi[2,3,*]

Abstract
Shorelines are vital and dynamic components of the coastal zone, constantly changing due to various environmental factors. These areas hold significant recreational, economic, and ecological importance, making the understanding of shoreline alterations critical. Unlike open oceans, the Caspian Sea (CS) has experienced a noticeable decline in water level since the late 1990s due to a combination of climatic variability, reduced riverine inflow, increased evaporation, and anthropogenic factors. This decline in water level is expected to drive morphological changes in the shorelines, with an overall trend of shorelines retreating seaward. In this study, the shoreline changes of Ogurja Island, the largest island in the CS, were analyzed using Sentinel-2 satellite imagery from 2015 to 2023, covering a total of 9 images, and the Digital Shoreline Analysis System tool. The study aimed to establish a relationship between these shoreline changes and the decline in the Caspian Sea water level (CSL). The results reveal a strong correlation, with shoreline movements reaching up to 80 m/year in some areas, and significant changes are expected with the projected CSL decline. This research offers an initial attempt to connect shoreline dynamics with water level fluctuations, highlighting the importance of considering shoreline changes in future water level predictions. The study recommends that future research focus on integrating advanced models, such as hydrodynamic simulations and machine learning techniques, to refine shoreline predictions and enhance understanding of the CS's dynamic coastal environment.

Keywords
Ogur Chinsky; Caspian Sea; Shoreline Changes; Decreasing Water Levels; DSAS

[1] *Faculty of Marine Science and Technology, University of Hormozgan, Bandar Abbas, Iran*
[2] *Center Providing Consultation and Simulation Services For Coastal And Marine Environments (NPDS Company), Bandar Abbas, Iran*
[3] *Physical Oceanography, Shahid Rajaee Port Complex, Ports and Maritime Organization, Bandar Abbas, Iran*
***Correspondence**: d.ghaderi@irseas.ir, danialghaderi1@gmail.com (D. Ghaderi)

Received: 30 July 2024; **revised:** 8 May 2025; **accepted**: 12 May 2025

1. Introduction

Coastal regions consist of areas where interactions among terrestrial, marine, and atmospheric systems occur simultaneously, leading to dynamism (Davidson-Arnott et al., 2019; Gunasinghe et al., 2021; Hsu et al., 2007). As a result, they are quickly impacted by human activities as well as fluctuations in climate, weather conditions, and natural hazards (Ghaderi and Rahbani, 2023; Johnston et al., 2023; Parthasarathy and Deka, 2019). Sometimes, these impacts are minor and seamlessly integrated into future dynamics, while at other times, they pose risks to both humans and the surrounding environment. In a study examining long-term changes in the shoreline of Hormuz Island, located in the semi-enclosed region of the Strait of Hormuz, it was found that the rate of change is minimal (0.1 m/year) and consistent with the low-energy hydrodynamic conditions of the area (Rahbani and Ghaderi, 2024). In contrast, short-term (seasonal) changes in the shoreline of the Tiab estuary on the northeastern coast of the Strait of Hormuz were significant, with changes ranging from 40 to 200 m (Rahbani et al., 2023a), primarily due to high-energy flood and ebb conditions (Ghaderi and Rahbani, 2021). Natural hazards can rapidly impact coastal areas, causing significant challenges. For example, the eruption of a mud volcano on Dashli Island in the southern Caspian Sea (CS) led to a 155% increase in the island's area within a very short period. This increase was caused by the emergence of a large volume of mud accompanying the eruption onto the island's surface (Ghaderi and Rahbani, 2022). In coastal areas, storms can occasionally exert immediate and significant impacts on shoreline changes. For instance, the study by Mishra et al. (2024) examined shoreline variations along Mocha in the coastal regions of Myanmar and Bangladesh. Over longer timescales, natural

hazards can also influence shoreline dynamics, with Sea Level Rise (SLR) being one example that poses a threat to coastal regions as a result of global warming. For instance, the study by Santos et al. (2024) on the shoreline of Conde County, Brazil, reveals a shoreline retreat rate of −0.27 m/year between 1985 and 2022. Weerasingha and Ratnayake (2022) and Mariotti and Hein (2022) conducted studies on SLR. A survey by Hossen and Sultana (2023) found erosion rates as high as 2.2 m/year on the shoreline of Saint Martin Island in the Bay of Bengal. Ghanavati et al. (2021) conducted research on the vulnerability of the Makran coast in the Gulf of Oman. The study highlights the vulnerability of coastal areas to SLR. Furthermore, Ghaderi and Rahbani (2024) showed that erosion is prevalent in the eastern regions of these areas.

In addition to the aforementioned studies, it is clear that the CS basin, which holds the title of being the largest lake globally, is undergoing a decline in water levels as a result of its enclosed nature, and given the influence of global warming, evaporation contributes significantly to this decline in water level (Chen et al., 2017; Lahijani et al., 2023b; Samant and Prange, 2023). The decline of the Caspian Sea water level (CSL) poses a significant threat to its coastal zones, leading to notable environmental and socio-economic challenges (Leroy et al., 2022). This phenomenon has resulted in shoreline retreat, intensified coastal accretion, and the degradation of coastal habitats. The retreating coastline disrupts ecosystems, particularly wetlands and marshes, which serve as critical habitats for diverse flora and fauna. This issue was also highlighted in the study by Haghani et al. (2016), which focused on the response of the Sefidrud Delta to fluctuations in the CSL. Data from Hydroweb from 1993 to 2022 indicates that the CSL has decreased at a rate of 5.4 cm/year (Chen et al., 2023). Undoubtedly, this decline in water level will have significant effects on coastal areas (Lahijani et al., 2023a). Kakroodi et al. (2014) conducted a study to investigate the response of the shoreline along the Iranian Caspian Coast to rapid sea-level changes in the 20th century. Their findings revealed that during the period of decreasing CSL from 1929 to 1977, the shoreline advanced seaward (around 120 m/year), exposing vast areas of the seabed. These changes were particularly pronounced in regions with high sediment deposition and low slope. Additionally, during the period after 1995, when the CSL remained relatively high until around 2001, shoreline change rates varied significantly depending on geographic location and local conditions. In most areas, shoreline retreat occurred, reaching several hundred m/year and even exceeding 1.7 km/year in shallow and lagoonal regions. Rezaee et al. (2022) reported that shoreline changes in the gently sloping coast of southern CS, particularly near Fereydounkenar Port, were influenced by water level decline, with about 260000 m^2 of accretion observed near the breakwater. Similarly, Isaie Moghaddam et al. (2021) utilized Digital Shoreline Analysis System (DSAS) tools and satellite imagery to illustrate substantial declines in Gorgan Bay and Gomishan Lagoon, which are attributed to the decrease in water level (with shoreline change rates ranging from 40 to 212 m/year). Hence, in this particular water basin, the dynamics of water level operate in a unique manner, unlike coastal areas located in oceans where rising sea levels primarily lead to erosion (landward movement of the shore). However, in the CS, the reduction in water level results in coastal areas experiencing accretion, or the seaward movement of the shoreline. While many studies have documented shoreline changes in various regions, the novelty of this study lies in its focus on quantifying the direct relationship between shoreline morphology and the declining CSL, specifically through the analysis of Ogurja Island in the southern CS. This research aims to contribute a unique perspective by linking shoreline dynamics with the observed decrease in water levels over a specific timeframe. Using Remote Sensing (RS) data, this study seeks to evaluate the rate and pattern of shoreline change as a response to water level fluctuations, providing new insights into how these environmental factors interact over short-term periods. By incorporating this new approach, the study not only enhances our understanding of coastal processes in the CS but also introduces an innovative method for a preliminary estimation of the declining CSL trend based on the forecasted future shoreline. Although additional statistical processes and more comprehensive datasets could enhance the robustness of the findings, this research addresses a gap in the existing literature, making contributions to the field of coastal morphology and its relationship with declining water level trends. In this approach, the forecasted future shoreline (derived from past trend behavior) can indicate the future CSL decline trend. While this estimation is subject to uncertainties, it can be considered reliable under the assumption that current hydrological and climatic conditions in the CS basin (such as temperature, evaporation, water inflow, etc.) persist.

2. Methods

2.1 Study area

The target area in this study is Ogurja Island, the largest island in the CS, also known as Ogur Chinsky. This island is located in the eastern part of the southern CS within the territorial jurisdiction of Turkmenistan and in proximity to the Cheleken Peninsula (Figure 1A and B). The island is narrow and elongated from north to south, with its maximum width being approximately 2.4 km and its maximum length around 37.5 km. Based on satellite images and news sources, the island is predominantly composed of low sand dunes covered with grass and bushes. Although there are no permanent residents, the island holds ecological importance, providing habitat for species like the endemic seal, Pusa caspica (Dmitrieva et al., 2016; Shirazi et al., 2023) and a variety of seabirds. Between 2015 and 2023, the

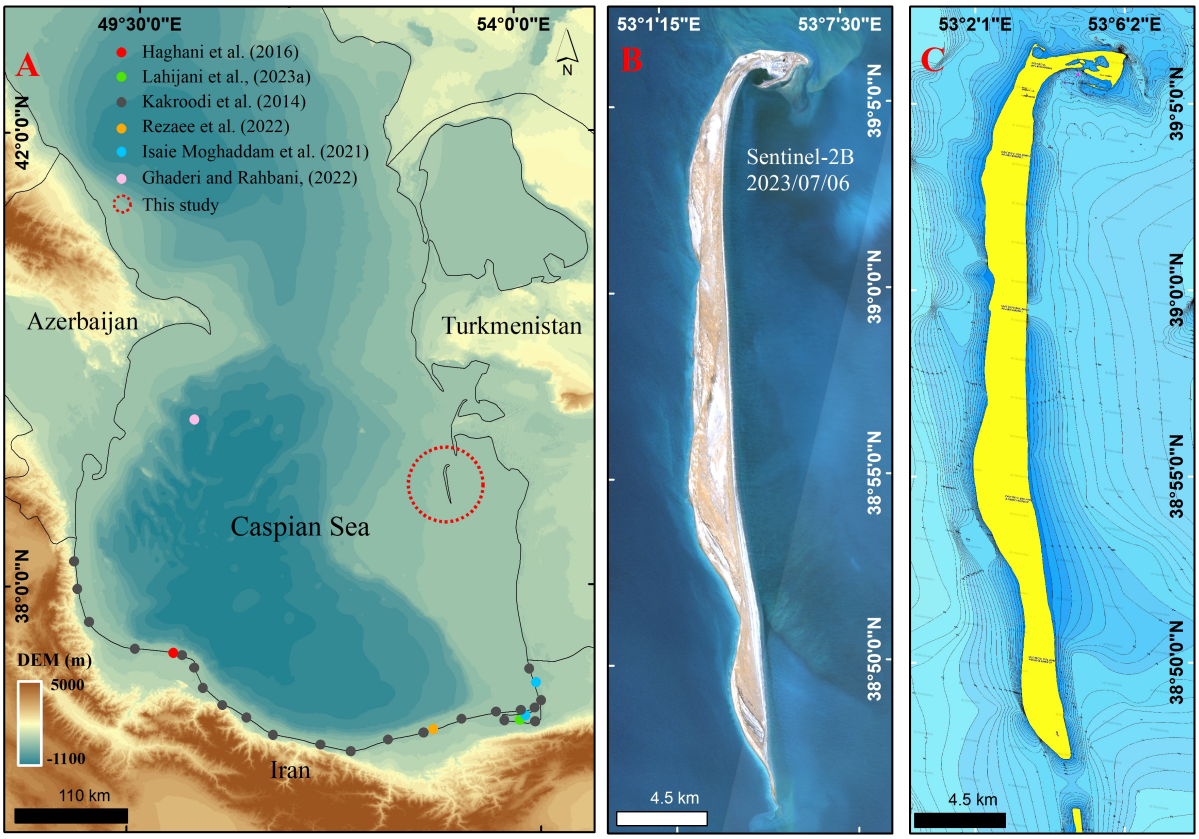

Figure 1. A) The geographical location of Ogurja Island, B) RGB satellite image from Sentinel-2, and C) Bathymetric map of the area surrounding the island, sourced from Navionics ChartViewer. Bathymetric isolines represent depth variations at one-meter intervals.

island's area grew from 53.9 km^2 to 59.9 km^2, indicating a 6 km^2 expansion over 9 years attributed to declining CSL. The marine area surrounding Ogurja Island, situated in the eastern part, has a shallower depth compared to the average depth of the southern CS. Prange et al. (2020) suggest that should the CSL decrease by 18 m by the close of the 21st century, this region will become completely dry. The bathymetric map of the island's vicinity is provided in Figure 1C (NAVIONICS, 2023). Ogurja Island features a simple, undeveloped coastline, allowing sediment deposition and transport processes to occur in a natural and undisturbed manner. In contrast, developed areas such as the Port of Beris, located on the northern coast of the Gulf of Oman (Ghaderi and Rahbani, 2020a), and Bandar Abbas city, situated on the north coast of the Strait of Hormuz (Ghaderi and Rahbani, 2020b), have experienced significant shoreline changes of up to 30 m/year due to the presence of coastal structures.

The CS, the largest enclosed inland water body on Earth, has undergone significant fluctuations in its water level over the past few decades (Haghani et al., 2016; Kakroodi et al., 2014; Roshan et al., 2012). Historical observations and satellite-based measurements indicate a general declining trend in the CSL since approximately 1995, accompanied by periodic fluctuations (Chen et al., 2017; Kakroodi et al., 2014). According to data obtained from the HYDROWEB database (Crétaux et al., 2011), the water level on September 27, 1992, was recorded at −26.48 m, while by August 20, 2023, it had dropped to −28.33 m (Figure 2B). This represents an overall decrease of 1.85 m over 31 years. Despite the long-term decline, short-term oscillations in water level are evident, reflecting the combined influence of climatic variability, riverine inflow, evaporation, and anthropogenic factors (Roshan et al., 2012). Understanding this dynamic behavior is crucial, as it directly impacts the ecological and socio-economic aspects of the Caspian region, including shoreline stability, habitat alteration, and regional water management strategies (Prange et al., 2020). To illustrate the long-term changes in Ogurja Island, Figure 2 has been prepared. This figure includes satellite imagery from Landsat 9 (dated 2023/07/02) and Landsat 5 (dated 1995/07/29), utilizing the near-infrared band for visual comparison (Figure 2A and C). Various parts of the island were narrower on 1995/07/29, when the CSL was approximately −25.92 m. For instance, section C2 represents a very narrow land strip. However, on 2023/07/02, with the CSL at −28.26 m, a significantly larger portion of Ogurja Island is exposed above water (see,

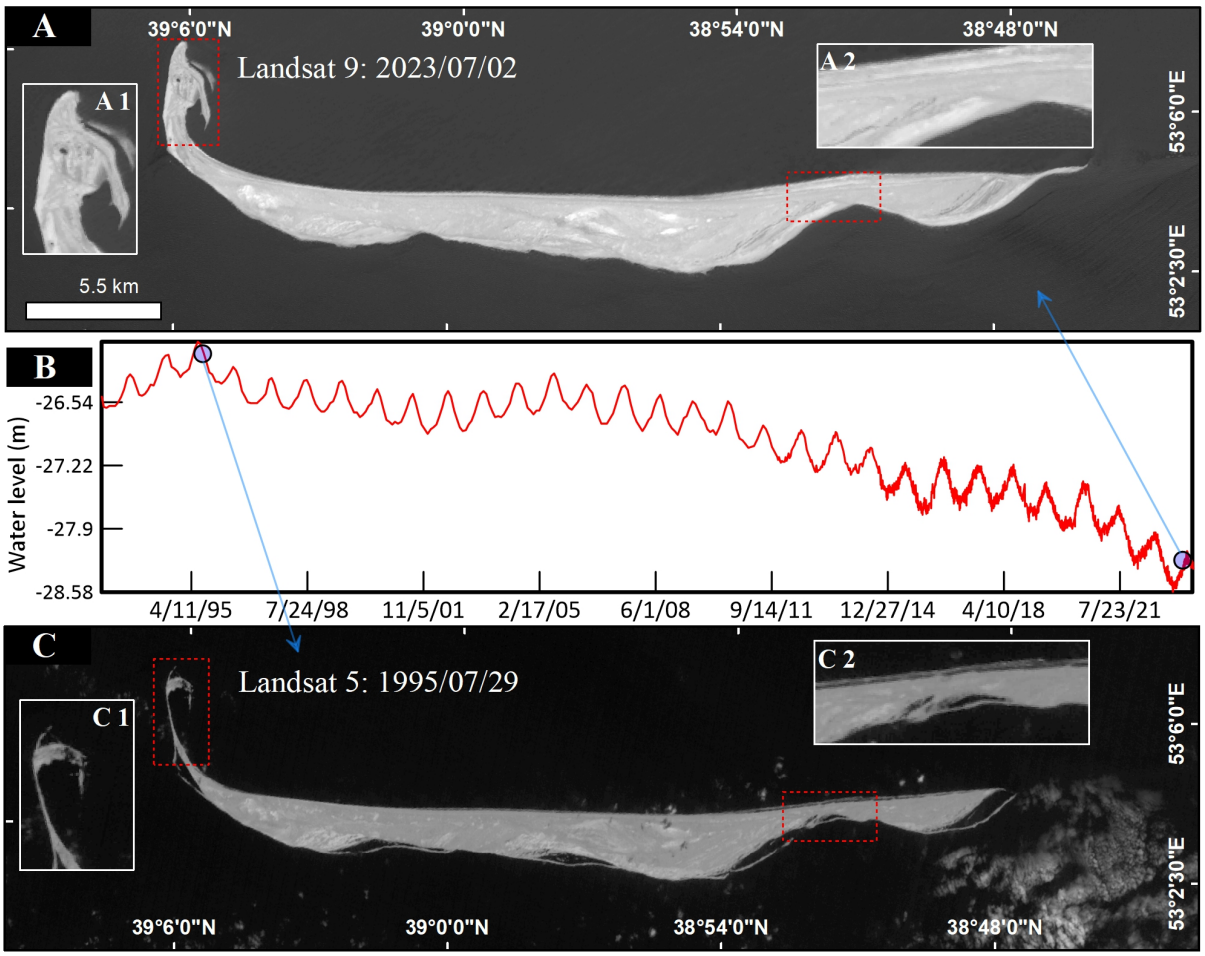

Figure 2. Long-term changes of Ogurja Island in relation to CSL variations. A) Near-infrared band image from Landsat 9 dated 2023/07/02, B) water level changes from 1992 to 2023, and C) near-infrared band image from Landsat 5 dated 1995/07/29.

for example, section A1). Therefore, based on the findings of studies by Samant and Prange (2023) and Kakroodi et al. (2014), it can be conclusively stated that since 1995, the declining CSL has significantly impacted the coastal regions.

2.2 Data collection and image processing

The satellite imagery utilized is sourced from Sentinel-2 A and B (ESA, 2020). These images span from 2015 to 2023, all captured during July and August (Table 1). It is noteworthy that all images are cloud-free, as confirmed through the metadata of Sentinel-2 products and further verified by meticulous manual and visual inspection to ensure data quality. The variation in water levels due to tides is a significant concern in these investigations (Boak and Turner, 2005; Ghaderi and Rahbani, 2020b; Rahbani et al., 2023a; Rahbani and Ghaderi, 2024); however, in the CS basin, tidal fluctuations are negligible. In Turkmen Bay, the maximum tidal range is approximately 21 cm, while in the western section of the South Caspian Basin, it falls within the range of 5–10 cm (Medvedev et al., 2020, 2017). Therefore, this study disregards the influence of tidal variations. The MSI sensor on the Sentinel-2 satellite captures images with a spatial resolution ranging from 10 to 60 m across 13 spectral bands ranging from 0.443 to 2.19 μm (Barsi et al., 2018). Only Band 3 (λ_G) and Band 8 (λ_{NIR}), with central wavelengths of 0.560 and 0.842 μm, respectively, are utilized. Pre-processing prerequisites for satellite images include geometric, radiometric, and atmospheric correction (Ghaderi and Rahbani, 2022, 2020a). While Sentinel-2's L1C products are geometrically and radiometrically adjusted (Gascon et al., 2017), they necessitate atmospheric correction. Several algorithms exist for conducting this correction. As outlined in the research literature (Ghaderi and Rahbani, 2022, 2020b; Pereira-Sandoval et al., 2019; Rahbani et al., 2023a; Rahbani and Ghaderi, 2024), the Case 2 Regional CoastColour algorithm (C2RCC), tailored for coastal settings (Brockmann et al., 2016), has been employed. This algorithm was chosen because it is specifically designed for coastal and marine environments and

Table 1. Satellite data images and bands information used in the NDWI index.

Year	Satellite	Date	Time	Sensor	Band used	Central wavelength (μm)	Pixel resolution (m)
2015	Sentinel-2A	2015/08/12	07:23	MSI	λ_G, λ_{NIR}	0.560, 0.842	10
2016	Sentinel-2A	2016/07/17	07:23	MSI	λ_G, λ_{NIR}	0.560, 0.842	10
2017	Sentinel-2B	2017/07/07	07:23	MSI	λ_G, λ_{NIR}	0.560, 0.842	10
2018	Sentinel-2B	2018/07/12	07:16	MSI	λ_G, λ_{NIR}	0.560, 0.842	10
2019	Sentinel-2A	2019/07/12	07:16	MSI	λ_G, λ_{NIR}	0.560, 0.842	10
2020	Sentinel-2A	2020/07/06	07:16	MSI	λ_G, λ_{NIR}	0.560, 0.842	10
2021	Sentinel-2B	2021/07/06	07:16	MSI	λ_G, λ_{NIR}	0.560, 0.842	10
2022	Sentinel-2A	2022/07/06	07:16	MSI	λ_G, λ_{NIR}	0.560, 0.842	10
2023	Sentinel-2A	2023/07/11	07:16	MSI	λ_G, λ_{NIR}	0.560, 0.842	10

is integrated within the SNAP application (Brockmann et al., 2016; Soriano-González et al., 2022). All necessary pre-processing has been completed using SNAP software. In this study, all processing steps were applied manually and in a controlled manner to the satellite data to ensure stability and avoid crashes, particularly given the resource limitations of a personal computer. Figure 3A displays the 2023 image following the implementation of the C2RCC algorithm.

2.3 Shoreline extraction

The optimal distinction between water and land features in satellite imagery has been accomplished through the application of McFeeters' proposed Normalized Difference Water Index (NDWI). This equation is a well-known and extensively utilized index that has been employed in numerous studies (Ghaderi and Rahbani, 2020a; Hossen and Sultana, 2023; Rahbani et al., 2023a; Rahbani and Ghaderi, 2024; Shamsaie and Ghaderi, 2025; Zambrano-Medina et al., 2023). Eq. 1 outlines the foundation of this index (McFEETERS, 1996).

$$NDWI = \left(\frac{\lambda_G - \lambda_{NIR}}{\lambda_G + \lambda_{NIR}}\right) \tag{1}$$

In this formula, λ_G and λ_{NIR} represent the green and near-infrared wavelength bands, respectively. The near-infrared band is highly absorbed by water and strongly reflected by land, making it an ideal band for differentiating between water and land features. Additionally, the green band is sensitive to the presence of suspended particles in the water, which further aids in distinguishing water from land. The combination of these two bands leverages their respective characteristics, allowing for the most accurate separation of water and land (Ghaderi and Rahbani, 2020b; McFEETERS, 1996; Pisanti et al., 2022). The outcome is a raster file with values ranging from -1 to $+1$, with values near $+1$ indicating the presence of water features and values near -1 indicating the presence of land features (Figure 3B) (Do et al., 2019; Ghaderi and Rahbani, 2025; Rahbani and Ghaderi, 2024).

The next step in shoreline extraction involves the creation of a two-class raster classification (e.g., Figure 3B). For this purpose, K-Means unsupervised classification has been utilized, as proposed in the studies by Ghaderi and Rahbani (2023), (2020a), Rahbani et al. (2023a), Rahbani and Ghaderi (2024), and Toure et al. (2019). The core principle of the K-means algorithm is to minimize the performance index of clusters, known as the square error, and an error criterion. It offers benefits such as conciseness, effectiveness, and rapid computation (Jumb et al., 2014; Rashmi et al., 2016). This approach is an error reduction algorithm that aims to minimize the sum of squared errors. The mathematical expression of the K-means function is depicted as Eq. 2 (Li and Wu, 2012).

$$e^2(K) = \sum_{k=1}^{K} \sum_{i \in C_k} (x_i - C_k)^2 \tag{2}$$

The outcome of K-Means unsupervised classification of images is depicted, for instance, in Figure 3C, comprising two segments: water and land features. Subsequently, the shorelines are extracted by delineating their borders (Figure 3D).

2.4 Shoreline analysis

The DSAS tool, created by the United States Geological Survey (Thieler et al., 2009), was utilized to statistically analyze shoreline alterations. Apart from offering drawing and calculation functions, this tool offers multiple indexes aiding in the assessment of shoreline changes. Utilizing this tool for analyzing shoreline changes is highly popular and effective. For instance, Ghaderi and Rahbani (2022) aimed to determine the impact of the eruption of the mud volcano on the area of Dashli Island; Rahbani et al. (2023) investigated short-term changes in the channels of Tiab estuary; Ghaderi and Rahbani (2023) analyzed the hydrodynamic processes involved in the construction of a port and

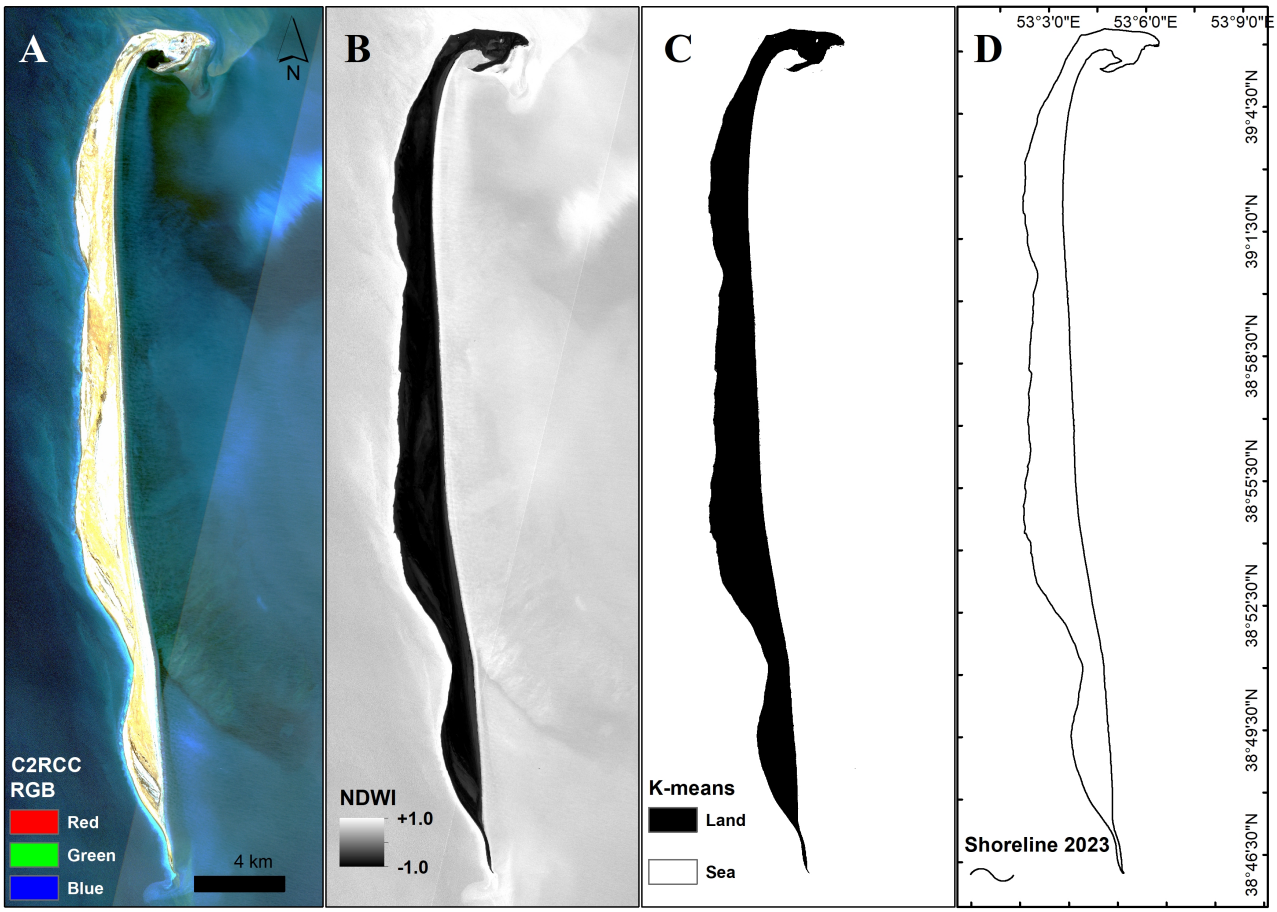

Figure 3. The pre-processing and processing stages of satellite images to extract shorelines. A) The RGB image of 2023 after applying the C2RCC algorithm. B) The output of NDWI. C) The two-class raster file derived from K-Means. D) The 2023 shoreline extraction.

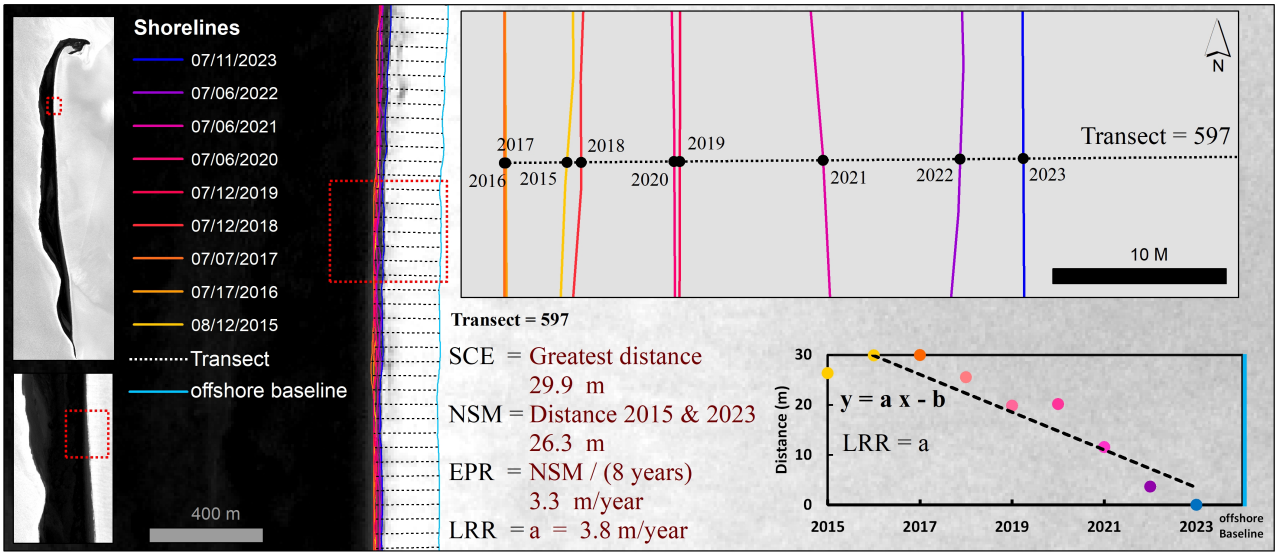

Figure 4. Schematic of the calculation of indexes; NSM, SCE, EPR, and LRR in Transect 597.

its effects on the shoreline; Rahbani and Ghaderi (2024) classified shoreline changes on an island located in a semi-enclosed water domain; Mageswaran et al. (2021) studied the effects of SLR on Little Andaman; and Hossen and Sul-

tana (2023) examined shoreline changes on Saint Martin Island in the oceanic region. They all utilized the DSAS tool for their respective analyses. The fundamental process of DSAS operation entails establishing a hypothetical baseline (in this research, an offshore baseline was implemented) and sketching transects at angles nearing perpendicularity to each shoreline (in this investigation, transects were generated at 10 m intervals) (Thieler et al., 2009). The method of shoreline changes has been analyzed using four indexes; Shoreline Change Envelope (SCE), Net Shoreline Movement (NSM), End Point Rate (EPR), and Linear Regression Rate (LRR). The functionality of each index is explained in Figure 4. The SCE calculates the greatest distance between shorelines along each transect; for instance, in transect 597, this index yields a value of 29.9 m. The NSM determines the distance between the oldest (2015) and youngest (2023) shorelines, which amounts to 26.3 m in transect 597. The EPR represents the ratio of the EPR value to the number of years; in transect 597, it stands at 3.3 m/year. While these three metrics rely on just two shorelines to gauge changes, LRR assesses shoreline alterations by considering all shorelines through linear regression. In transect 597, the LRR value is 3.8 m/year (Figure 4). As mentioned in the description of the metrics, the SCE and NSM quantify the extent of change, whereas the EPR and LRR ascertain the rate of change.

Detecting shoreline changes through RS methods always accompanies inherent sources of error, which define the level of uncertainty. Focusing on error sources and their identification will result in decreased uncertainty. According to the research conducted by Godwyn-Paulson et al. (2021) and Ayadi et al. (2016), error origins encompass seasonal error (E_s), tidal fluctuations error (E_t), digitizing error (E_d), rectification error (E_r), and pixel error (E_p),

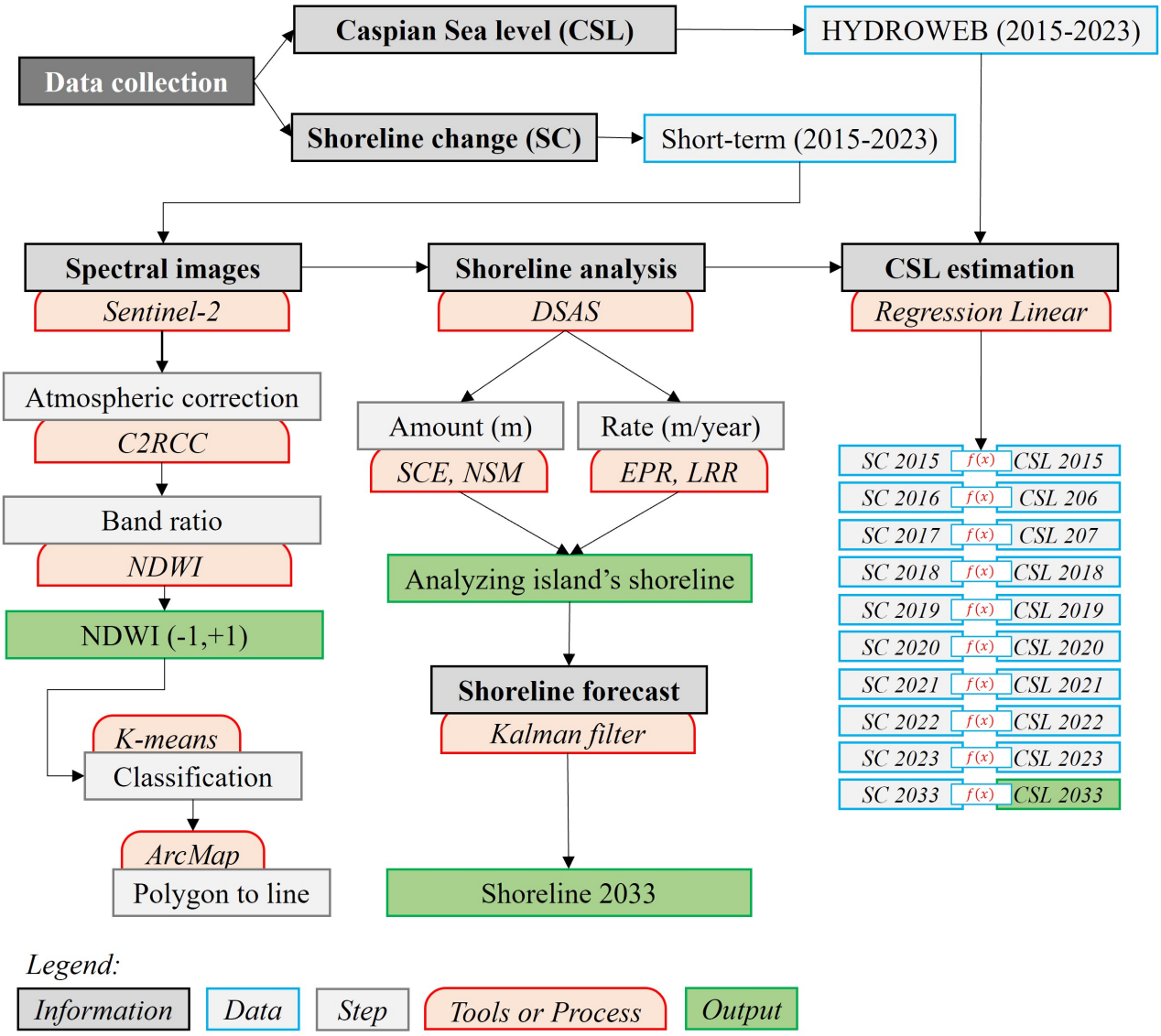

Figure 5. Workflow of the study methodology.

determined through Eq. 3.

$$Unc = \sqrt{\left(E_s^2 + E_t^2 + E_d^2 + E_r^2 + E_p^2\right)} \quad (3)$$

All selected satellite images pertain to July and August (see Table 1), with similar climatic conditions and minimal water level fluctuations (negligible tide). Hence, E_s and E_t are insignificant. Considering identical orthorectification and spatial resolution, E_r and E_p can be disregarded. Moreover, E_d is logically related to the pixel size of the images, which is equivalent to 10 m (Vallarino Castillo et al., 2022; Yum et al., 2023). Therefore, error sources are solely associated with the pixel size of the images and potential water level fluctuations (excluding tide). In this study, the estimated value for uncertainty is approximately 10 m. Santos et al. (2021) provided an estimation of the overall uncertainty within a range of ± 15.3 to ± 7.7 m, and Nassar et al. (2019) estimated it to be around ± 37 m. Due to the consistent decline in the CSL (Chen et al., 2023; Lahijani et al., 2023b; Samant and Prange, 2023), estimated changes are impacted by these fluctuations.

Furthermore, the uncertainty associated with the rate at which the shoreline changes is calculated based on Eq. 4 (Rajasree et al., 2016; Santos et al., 2021). In each transect along the shoreline, U represents the level of uncertainty. The total number of shorelines being examined is represented by n. $year_n$ refers to the most recently obtained shoreline, while $year_1$ represents the year of the initially extracted shoreline (Rajasree et al., 2016).

$$U = \frac{\sqrt{U_1^2 + U_2^2 ... U_n^2}}{year_n - year_1} \quad (4)$$

The uncertainty has been computed for each transect, yielding an average uncertainty of around ± 1.5 m/year. Santos et al. (2021) determined the uncertainty for the endpoint rate to be approximately ± 0.7 m/year, and Nassar et al. (2019) indicated a range of ± 5.9 to ± 1.4 m/year.

The DSAS tool also has the capability to predict future shoreline positions. This prediction is based solely on the historical behavior of shorelines (Seenath, 2022). The predictive principles of this tool are based on the statistical Kalman filter model (Himmelstoss et al., 2018). This model relies on a set of linear regression rates to forecast the future position of a shoreline (Yan et al., 2021). Due to the influence of multiple variables on shoreline changes, the Kalman filter model may have some susceptibility to errors. However, it does provide an initial and quick estimate for planners, policymakers, and managers (Nijamir et al., 2023). In this particular study, which assumes a continuous and linear decrease in the CSL, this factor itself will be reflected in shoreline changes. Therefore, there should be a significant correlation between changes in the CSL and shoreline changes. Therefore, in this study, based on the analysis of shoreline changes, the shoreline position of the island has been estimated for the next ten years (2033). Ultimately, the fluctuations in the shoreline of Ogurja island between 2015 and 2023 have been assessed in relation to the CSL data sourced from HYDROWEB (Crétaux et al., 2011). The entire methodology of this study is illustrated in the workflow presented in Figure 5.

3. Results and discussion

3.1 Analyzing the island's shoreline

The changes in the shoreline of Ogurja Island from 2015 to 2023, as indicated by four metrics (SCE, NSM, EPR, and LRR), are presented in Figure 6. The SCE determines the maximum changes occurring in the island's shoreline. As illustrated in Figure 6A, it is apparent that the eastern portion of the island undergoes more pronounced modifications compared to the western side. The maximum changes in this section can be attributed to the depth and slope of this area (Figure 1C). In the western part, significant changes in the shoreline occur specifically in those regions characterized by bends (such as boxes *b* and *d* in Figure 6A). The NSM determines the type of changes occurring. As depicted in Figure 6B, the eastern portion shows changes that are predominantly directed seaward, with the highest observed in box *h*. Based on the bathymetric data surrounding the island, it can be observed from Figure 1C that box *h* exhibits the lowest slope. As a result, this particular section will be significantly impacted by the declining CSL. In the western section, the majority of shoreline changes are directed seaward, while only small areas exhibiting a landward movement, particularly in regions where the coast curves, such as section c.

By comparing the SCE and NSM, we can gain insights into changes in the shoreline. Figure 7 illustrates a linear comparison of the two indexes, with a correlation coefficient of 0.84. The high level of similarity between the two indexes suggests that the majority of the shoreline has undergone a linear seaward change as the CSL has decreased. This trend is observed throughout most areas, with the exception of a few small regions like box *c* in Figure 7. Furthermore, it is evident from Figure 7 that both lines exhibit a completely linear pattern. However, there is a distinction in box *h*, indicating that the oldest shoreline (2015) has experienced less change compared to more recent years. Despite the predominant seaward changes of shoreline, the shoreline behavior is not linear.

The rate of shoreline changes, as indicated by the EPR and LRR indexes, corresponds with SCE and NSM but provides a clearer understanding of the changes over time. As illustrated in Figure 8, the changes in the blue line (EPR) exhibit a high correlation with those in the red line (LRR), with a correlation coefficient 0.96. In several regions, they align closely, while noticeable differences are observed in some specific areas, such as boxes *f* and *h*. This indi-

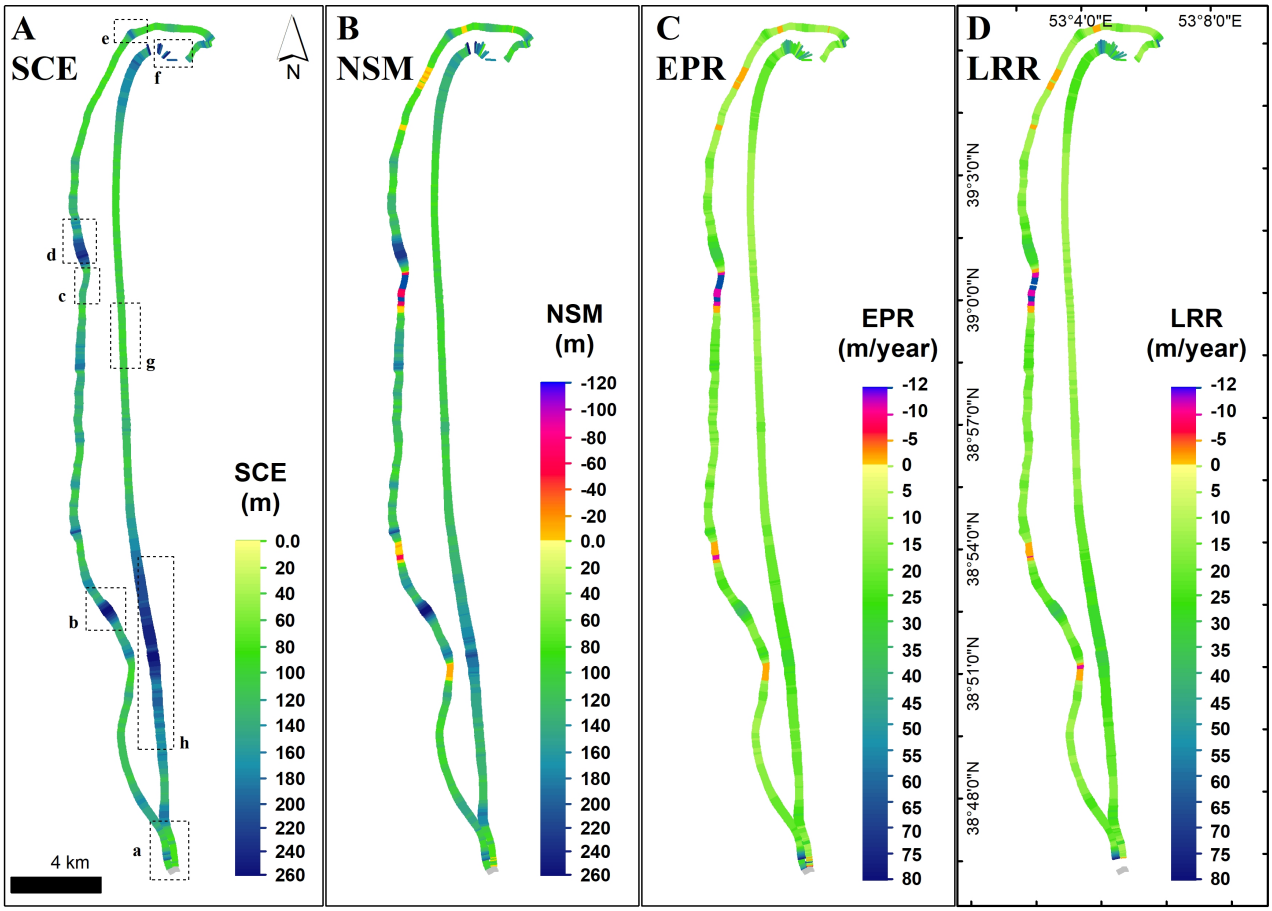

Figure 6. Shoreline changes of Ogurja Island according to A) SCE, B) NSM, C) EPR, and D) LRR indexes.

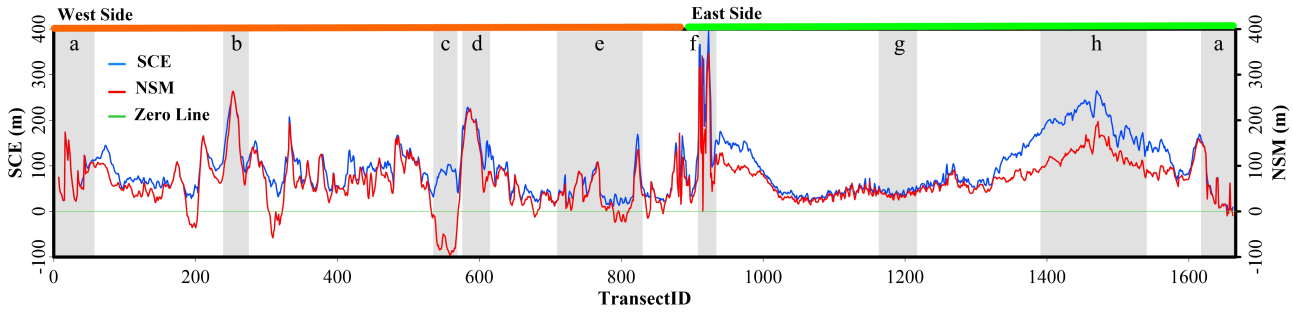

Figure 7. The shoreline changes of Ogurja Island are depicted by the SCE (blue line) and NSM (red line) indexes.

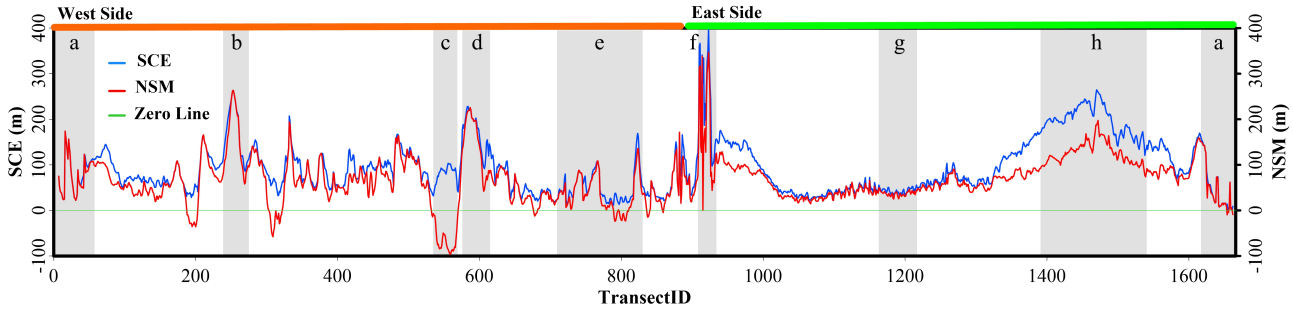

Figure 8. The shoreline changes of Ogurja Island are depicted by the EPR (blue line) and LRR (red line) indexes.

cates that the changes in most shorelines have been linear, except for box *h*. Therefore, it can be concluded that the short-term changes (2015–2023) in Ogurja Island align completely with the trend of the CSL. The southern narrow strip of the island (box *a*) exhibits the highest rate of change, reaching up to 80 m/year. Following that, in box *f*, located in the north of the island, the rate is approximately 50 m/year; this area is shallow and estuarine. In box *b*, changes occur at a rate of around 35 m/year, indicating that alterations in this area result from successive cycles of erosion and accretion (refer to the northern and southern parts of box *b* in Figure 6D). The extensive range of box *h* also experiences changes at a rate of 25 m/year; in the nearshore section of this box, there exists a shallow area (refer to Figure 1C). Therefore, in conclusion, short-term shoreline changes on the island are influenced by the decrease in the water level, although in some areas, hydrodynamic mechanisms and geomorphic features play a more significant role.

Different factors and origins in each aquatic environment can lead to distinct shoreline changes. For instance, the eruption of the mud volcano on Dashli Island in the CS caused significant alterations to the island within a few days (Ghaderi and Rahbani, 2022). Similarly, severe storms can have an immediate impact, as observed in Mishra et al. (2024), while natural disasters such as earthquakes can reshape the shoreline in less than a day, as demonstrated by Rahbani et al. (2023b). However, in the CS, the primary concern is the decline in CSL, which has led to long-term shoreline changes, predominantly in the form of accretion (seaward movement). As reported in our study, the short-term decline in the CSL (2015–2023) has resulted in the seaward movement of the shoreline (accretion), posing environmental risks to the region. Additionally, Haghani et al. (2016) study on the Sefidrud Delta (southern CS coast) has highlighted sediment accumulation. Other studies, such as Lahijani et al. (2023a), Kakroodi et al. (2014), Rezaee et al. (2022), and Isaie Moghaddam et al. (2021), which focus on the southern CS coast (Figure 1A), have also reported seaward movement of the shoreline.

Ogurja Island, influenced by declining water levels, has exhibited shoreline changes of up to 260 m (in the SCE index). These findings emphasize the significance of shoreline type and dominant environmental processes in determining the magnitude of shoreline modifications. This level of shoreline change may be observed in estuarine environments, such as Rahbani et al. (2023a), even though the CS is an enclosed body of water, it experiences high rates of accretion. Currently, due to SLR, most coastlines adjacent to oceans are facing the threat of erosion, which has garnered significant attention due to its direct impact on human communities and socio-economic interests, as highlighted in studies by Mariotti and Hein (2022) and Weerasingha and Ratnayake (2022). However, the situation in the enclosed CS is quite different, with a serious decline in water levels. In this context, the seaward advance of the shoreline poses a potential threat, the socio-economic and environmental impacts of which may not become immediately apparent. This warrants special attention from coastal managers and policymakers.

3.2 Analyzing the future of the island's shoreline

Due to the findings from the analysis of indexes, which have shown linear alterations in most of Ogurja Island's shoreline, the shoreline's position has been forecasted for the upcoming decade employing the Kalman filter model. The comparison between the position of the shoreline in 2033 and those in 2015 and 2023 is shown in Figure 9. The position of the 2033 shoreline is estimated based on the assumption of linear changes in the shoreline from 2015 to 2023. Therefore, if the decline in the CSL continues under the current conditions, the findings presented regarding the future shoreline forecast and the estimation of CSL changes can be considered reliable. As Yan et al. (2021) have noted, the Kalman filter, which is based on statistical methods, requires a set of linear regression rates for initialization in order to accurately predict future shoreline positions. Therefore, if past shorelines are provided with sufficient precision, the performance of the Kalman filter is expected to be reliable. This approach has been employed in studies such as those by Alharbi et al. (2023), Murray et al. (2023), and Khakhim et al. (2024). Shoreline forecasting performance is inherently associated with uncertainty (Khakhim et al., 2024; Yan et al., 2021). In this study, the uncertainty was found to be lower than the spatial resolution of the satellite pixel data. Therefore, despite the possibility that environmental factors may alter the linear process of shoreline changes in the future, the forecast uncertainty remains within an acceptable level. Hence, it can be concluded that over the next decade, the shoreline of the island will undergo changes of up to 300 m (or 30 m/year), and the land features will continue to emerge. The most significant changes are observed in boxes *b*, *d*, and *h* (Figure 10). In box *c* and the northern and southern parts of box *b*, changes occur in a landward manner, with a maximum amount of 150 m (or 15 m/year).

The eastern part of the island, which predominantly has shallower depths, clearly demonstrates being heavily influenced by the trend of decreasing CSL. Therefore, it can be inferred that shallow coastal areas of the CS are entirely susceptible to this declining trend in water level. According to a study conducted by Isaie Moghaddam et al. (2021), there has been a significant decrease in the size of Gorgan Bay and Gomishan Lagoon. Gorgan Bay has experienced a reduction in its area from approximately 523 km^2 in 1998 to around 372 km^2 in 2015, and Gomishan Lagoon has decreased from 148 km^2 in 1994 to approximately 50.5 km^2 in 2015. Moreover, Lahijani et al. (2023a) highlighted in their study that the decline in the CSL poses a significant threat to the drying of certain areas

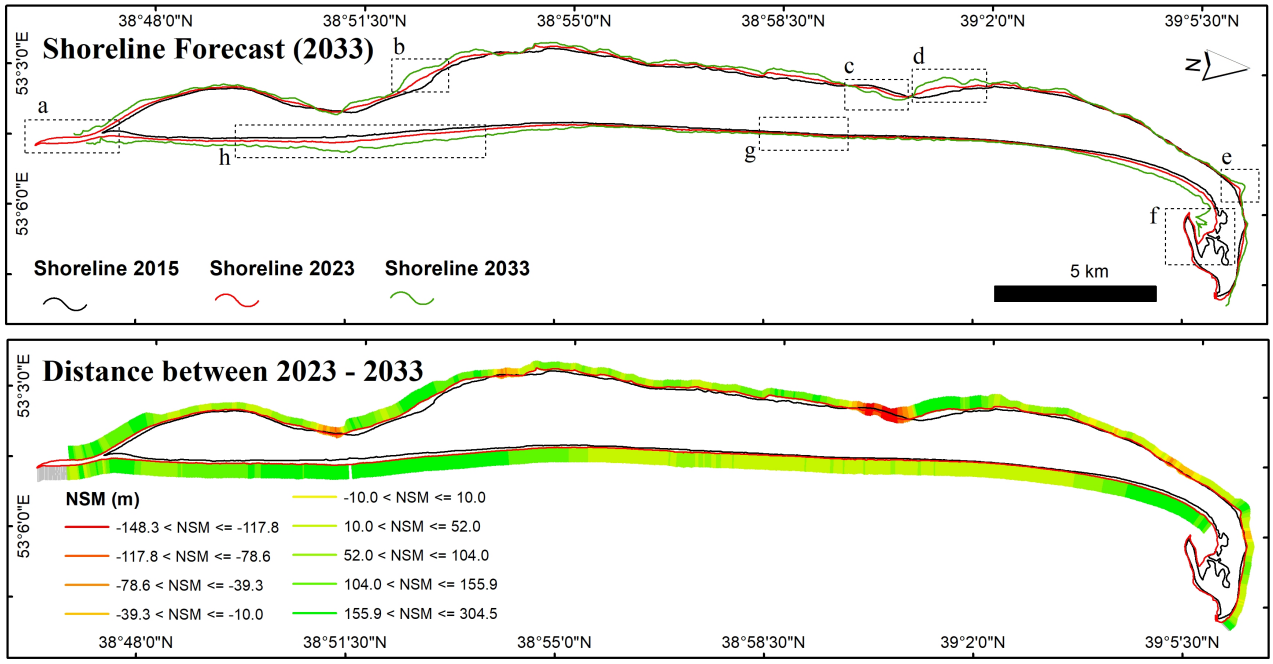

Figure 9. The shoreline forecast for Ogurja Island in 2033, A) The positions of three shorelines in 2015 (black line), 2023 (red line), and 2033 (green line), and B) The distance between the shorelines in 2023 and 2033.

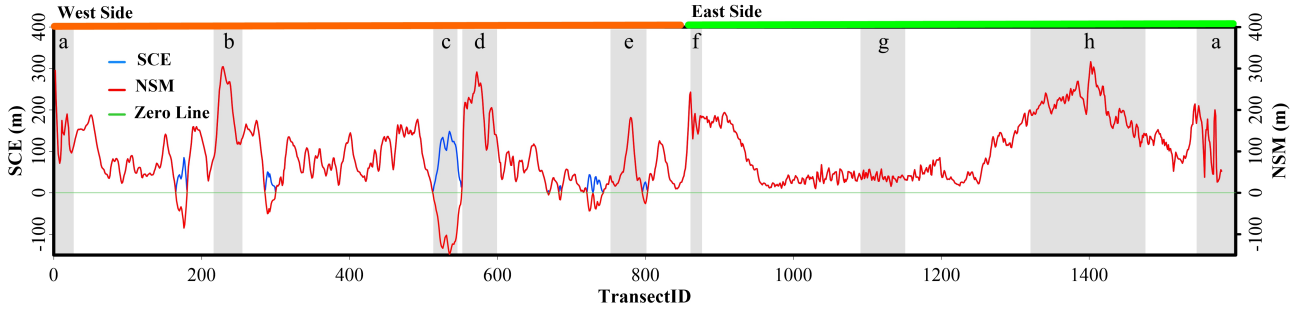

Figure 10. The shoreline changes of Ogurja Island between 2023 and 2033 in two SCE (blue line) and NSM (red line) indexes.

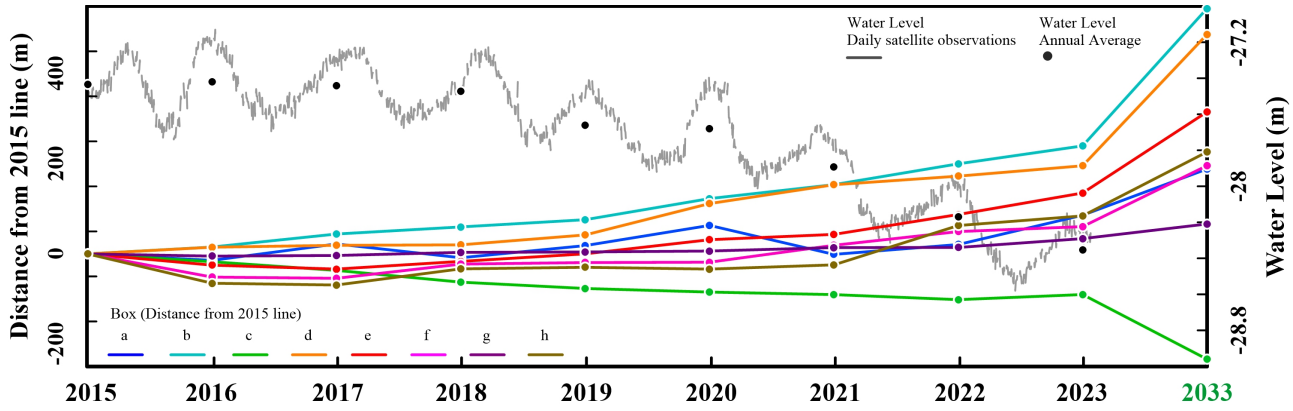

Figure 11. Average shoreline changes from 2015 to 2033 in eight boxes and CSL changes from 2015 to 2023.

in Gorgan Bay. As a result, the ongoing trend of declining CSL, particularly in landforms such as bays and lagoons, poses a significant environmental threat. In a separate study conducted by Rezaee et al. (2022), an analysis of the long-term changes in the shoreline of Fereydounkenar in the southern CS revealed a significant accretion. This accretion was directly attributed to the decrease in the CSL, rather than being influenced by hydrodynamic processes. Additionally, a study conducted by Toorani et al. (2021) revealed that the fluctuations in the Tajan region's shoreline are influenced by the declining CSL. However, in the Sefidrud, other hydrodynamics play a more role in the observed changes. According to a study on the coastal wetlands in the Sefidrud Delta conducted by Haghani et al. (2016) sediment deposition and the effects of human intervention have played a crucial role in shaping the rapid accretion of the delta.

By comparing the CSL and changes in the shoreline of Ogurja Island, a clear significant correlation is evident. In Figure 11, changes in the shoreline of eight selected boxes of the island from 2015 (as a reference) to 2023 and the prediction for 2033 are illustrated. Except for box *c*, which has moved landward, the rest of the boxes are seaward, essentially responding to the trend of decreasing CSL. Table 2 includes the correlation coefficient between the annual average water level and the rate of shoreline changes. Notably, there is a significant correlation in boxes *b*, *d*, *e*, *f*, *g*, and *h*, indicating a strong relationship. Hence, for the purpose of gaining a preliminary understanding of the correlation between water level and shoreline response, a linear regression equation has been established in this research. Therefore, considering the declining trend of CSL from 2015 to 2023 and the estimated shoreline change rates, an attempt has been made to provide an insight into the extent of future CSL decline. To achieve this, the shoreline position of the island in 2033 was first estimated using the Kalman filter. Subsequently, based on the linear regression between the variables, the future CSL decline was projected (as shown in Table 2). This estimation suggests a decline range of 4.8 to 11.4 cm/year. It is worth noting that the response of the shoreline to CSL fall may exhibit a time lag, a phenomenon associated with sedimentation and sediment transport processes (Ataei H. et al., 2018; Kakroodi et al., 2014). However, given the absence of complex coastal systems (such as marine structures) in the Ogurja Island region, this time lag is expected to be negligible. The more likely range of values is between 9.3 to 11.4 cm/year, as determined by the R-squared value. Zanganeh and Chaji (2024) have stated that the CSL is projected to decrease by 4.5 cm by the year 2024, according to the PSO-ANFIS model. In a study conducted by Chen et al. (2017) it was found that between 1996 and 2015, the CSL experienced an average annual decrease of approximately 6.72 cm, primarily due to evaporation, which is the main factor associated with global warming. Also, the linear trend estimates from Hydroweb data indicate an annual decrease in the CSL of 5.37 cm (Chen et al., 2023).

Future predictions of the CSL have proposed various approaches, and here, some studies are presented to provide insight into the future status. A prediction was put forward by Renssen et al. (2007), suggesting that the water level will undergo changes of 4 and 2 m respectively on centennial and decadal scales. Elguindi and Giorgi made predictions about the CSL for the 21st century based on global climate change simulations. Their findings indicate that increased evaporation at the sea surface causes a 9 m decrease in the CSL by the end of the century. Prange et al. (2020), in an effort to highlight the significance of reducing the CSL and the lack of attention from international policies, published a eport. The figure they presented reveals that a 9 m decrease in water level would result in substantial portions of the northern CS, Kara Bogas Gol, Gomishan Lagoon, Gorgan Bay, and nearshore areas becoming dry. Moreover, if the CSL were to decrease by 18 m, areas near Turkmenistan's sea and Ogurja Island would become completely dry.

3.3 Limitations and future research directions

Identifying the limitations of this study provides valuable insight into its constraints while highlighting potential directions for future research to advance knowledge in this field. One of the primary limitations of this research is the lack of access to high-resolution aerial imagery. Sentinel-2 satellite data was utilized as the best available option due to its extensive temporal coverage. However, the spatial resolution of these satellite products introduces uncertainties in shoreline identification, particularly in areas experiencing small-scale and dynamic shoreline changes. Moreover, the shoreline forecast method employed in this study relies solely on a linear approach based on historical shoreline data. This method does not incorporate hydrodynamic processes, hydro-morphological changes, or climatic factors, which play a crucial role in shoreline dynamics. Future studies could integrate numerical models to achieve more precise shoreline forecasts, provided that key environmental data, such as the rate of CSL decline, are accurately modeled. However, these projections are also associated with uncertainties arising from climatic modeling efforts. Additionally, a linear regression approach was used to establish the relationship between shoreline changes and the CSL decline. While effective, this method could be further refined by employing advanced techniques such as deep learning models, which may provide higher accuracy. However, deep learning models require larger and more comprehensive datasets. Future research is encouraged to incorporate all suitable Sentinel-2 images, available every five days, alongside daily CSL data as inputs for training deep learning models. This approach would ensure the inclusion of seasonal fluctuations in CSL, which were not fully accounted for in the current study. Recognizing these limi-

Table 2. Statistical information on the relationship between the average shoreline changes and the annual average CSL, and the linear regression forecasting of the water level in 2033.

box	Correlation	Regression	R2	CSL	
	coefficient	Linear Formula		2033 (m)	rate (cm/year)
a	-0.61	$y = -0.0066x - 27.589$	0.41	-28.83	-4.8
b	-0.98	$y = -0.004x - 27.317$	0.94	-29.50	-11.4
c	0.79	$y = 0.0074x - 27.264$	0.60	-28.99	-6.4
d	-0.95	$y = -0.0042x - 27.38$	0.91	-29.43	10.7
e	-0.98	$y = -0.006x - 27.577$	0.95	-29.47	-11.2
f	-0.98	$y = -0.0078x - 27.756$	0.84	-29.28	-9.3
g	-0.94	$y = -0.0271x - 27.519$	0.89	-29.32	-9.7
h	-0.96	$y = -0.0057x - 27.793$	0.77	-29.08	-7.3

tations provides a framework for refining methodologies and offers a roadmap for future investigations to improve the precision of shoreline change and CSL predictions.

4. Conclusions

This study investigates the use of RS images, specifically Sentinel-2 satellite data, to analyze shoreline changes around Ogurja Island in response to the declining CSL. The research focuses on understanding short-term shoreline changes and assessing how these changes correlate with water level fluctuations. Sentinel-2 data, with its extensive temporal coverage, has provided valuable insights into shoreline dynamics, allowing for the detection of significant shoreline shifts, including seaward movements with maximum changes reaching up to 80 m/year. The results reveal a strong correlation between shoreline changes and the decline in the CSL, with some areas showing a negative correlation of -0.98. This demonstrates the potential of using RS technology to track shoreline dynamics in response to environmental changes such as sea level decline. The DSAS tool further facilitated the quantification of these changes, offering a precise measure of both the rate and extent of shoreline movement. In terms of future projections, the Kalman filter model, based on a linear extrapolation approach, has been used to forecast shoreline changes up to 2033, based on observed trends from 2015 to 2023. These predictions provide important insights for understanding the potential future impacts of water level fluctuations on the shoreline of Ogurja Island. When shorelines face significant vulnerability — such as in the enclosed Caspian Sea — having rapid and accessible approaches, even with approximate estimations, is crucial for informing policymakers and coastal managers about potential risks. Therefore, based on the observed shoreline response from 2015 to 2023, we anticipate that CSL will decline by at least 4.8 to 11.4 cm/year over the next decade. Notably, this projected decline is consistent with findings from statistical analyses and other climate modeling studies. While RS images provide a cost-effective and timely method for monitoring shoreline changes, several limitations must be acknowledged. The spatial resolution of Sentinel-2 imagery, although high for many applications, introduces uncertainties, particularly in areas experiencing small-scale and rapid shoreline changes. Additionally, the reliance on linear models, such as the regression analysis used in this study, may not fully capture the complex hydrodynamic processes, morphological changes, and climatic factors that influence shoreline dynamics. Looking forward, integrating RS data with more advanced models that account for these factors could improve the accuracy of shoreline change predictions. The Kalman filter model used to forecast shoreline changes up to 2033 is a step in this direction, but future studies should explore the potential of combining satellite imagery with numerical hydrodynamic models to better capture the multifaceted nature of shoreline responses. In conclusion, while RS images, particularly from Sentinel-2, offer a powerful tool for analyzing shoreline changes and understanding the effects of CSL decline, the approach could benefit from further refinement. Future research should explore the integration of higher-resolution imagery, advanced modeling techniques, and more comprehensive environmental data to enhance the accuracy and reliability of shoreline change predictions.

Authors' contribution

Rahimeh Shamsaie: Conceptualization, Validation, Formal analysis, Investigation, Resources, Data curation, Visualization, and Writing — original draft. Danial Ghaderi: Conceptualization, Methodology, Writing — review and editing, Supervision, and Project administration. All authors have read and agreed to the published version of the manuscript.

Declaration of interest

None declared.

Data availability statement

The datasets generated and analysed during the current study are available and can be handed in on request.

References

Alharbi, O.A., Hasan, S.S., Fahil, A.S., Mannaa, A., Rangel-Buitrago, N., Alqurashi, A.F., 2023. *Shoreline change rate detection applying the DSAS technique on low and medium resolution data: Case study along Ash Sh'aybah-Al Mujayrimah coastal Area of the Eastern Red Sea, Saudi Arabia*. Reg. Stud. Mar. Sci. 66, 103118. https://doi.org/10.1016/j.rsma.2023.103118

Ataei H., S., Adjami, M., Neshaei, S.A., 2018. *The Effects of Sea Level Fall on the Caspian Sea Shoreline Changes*. Int. J. Coast. offshore Eng. 2, 1–12. https://doi.org/10.29252/ijcoe.2.3.1

Ayadi, K., Boutiba, M., Sabatier, F., Guettouche, M.S., 2016. *Detection and analysis of historical variations in the shoreline, using digital aerial photos, satellite images, and topographic surveys DGPS: case of the Bejaia bay (East Algeria)*. Arab. J. Geosci. 9, 26. https://doi.org/10.1007/s12517-015-2043-9

Barsi, J.A., Alhammoud, B., Czapla-Myers, J., Gascon, F., Haque, M.O., Kaewmanee, M., Leigh, L., Markham, B.L., 2018. *Sentinel-2A MSI and Landsat-8 OLI radiometric cross comparison over desert sites*. Eur. J. Remote Sens. https://doi.org/10.1080/22797254.2018.1507613

Boak, E.H., Turner, I.L., 2005. *Shoreline Definition and Detection: A Review*. J. Coast. Res. 214, 688–703. https://doi.org/10.2112/03-0071.1

Brockmann, C., Doerffer, R., Peters, M., Kerstin, S., Embacher, S., Ruescas, A., 2016. *Evolution of the C2RCC neural network for Sentinel 2 and 3 for the retrieval of ocean colour products in normal and extreme optically complex waters*. ESASP 740, 54.

Chen, J., Cazenave, A., Wang, S.-Y., Li, J., 2023. *Caspian Sea Level Change Observed by Satellite Altimetry*. Remote Sens. 15, 703. https://doi.org/10.3390/rs15030703

Chen, J.L., Pekker, T., Wilson, C.R., Tapley, B.D., Kostianoy, A.G., Cretaux, J. -F., Safarov, E.S., 2017. *Long-term Caspian Sea level change*. Geophys. Res. Lett. 44, 6993–7001. https://doi.org/10.1002/2017GL073958

Crétaux, J.-F., Arsen, A., Calmant, S., Kouraev, A., Vuglinski, V., Bergé-Nguyen, M., Gennero, M.-C., Nino, F., Abarca Del Rio, R., Cazenave, A., Maisongrande, P., 2011. *SOLS: A lake database to monitor in the Near Real Time water level and storage variations from remote sensing data*. Adv. Sp. Res. 47, 1497–1507. https://doi.org/10.1016/j.asr.2011.01.004

Davidson-Arnott, R., Bauer, B., Houser, C., 2019. *Introduction to Coastal Processes and Geomorphology*. Cambridge Univ. Press. https://doi.org/10.1017/9781108546126

Dmitrieva, L., Jüssi, M., Jüssi, I., Kasymbekov, Y., Verevkin, M., Baimukanov, M., Wilson, S., Goodman, S., 2016. *Individual variation in seasonal movements and foraging strategies of a land-locked, ice-breeding pinniped*. Mar. Ecol. Prog. Ser. 554, 241–256. https://doi.org/10.3354/meps11804

Do, A.T.K., Vries, S. de, Stive, M.J.F., 2019. *The Estimation and Evaluation of Shoreline Locations, Shoreline-Change Rates, and Coastal Volume Changes Derived from Landsat Images*. J. Coast. Res. 35, 56. https://doi.org/10.2112/JCOASTRES-D-18-00021.1

ESA, 2020. *Copernicus Open Access Hub of the ESA*. https://scihub.copernicus.eu/ (accessed 8.2.20).

Gascon, F., Bouzinac, C., Thépaut, O., Jung, M., Francesconi, B., Louis, J., Lonjou, V., Lafrance, B., Massera, S., Gaudel-Vacaresse, A., Languille, F., Alhammoud, B., Viallefont, F., Pflug, B., Bieniarz, J., Clerc, S., Pessiot, L., Trémas, T., Cadau, E., De Bonis, R., Isola, C., Martimort, P., Fernandez, V., 2017. *Copernicus Sentinel-2A calibration and products validation status*. Remote Sens. https://doi.org/10.3390/rs9060584

Ghaderi, D., Rahbani, M., 2025. *A Long-Term Survey on the Shoreline Changes of Gulf of Oman Coasts (Makran)*. Ocean Sci. J. 60, 11. https://doi.org/10.1007/s12601-025-00208-y

Ghaderi, D., Rahbani, M., 2024. *Evaluating the shoreline vulnerability of eastern coast of Makran employing geomorphological and hydrodynamic parameters*. J. Earth Syst. Sci. 133, 48. https://doi.org/10.1007/s12040-024-02266-7

Ghaderi, D., Rahbani, M., 2023. *Simultaneous employment of hydrodynamical simulation and RS imageries for analyzing the influence of an anthropogenic construction on shoreline transformation*. J. Hydraul. Struct. 9, 14–31.

Ghaderi, D., Rahbani, M., 2022. *Mud volcano as a feature of emergence in Caspian Sea*. Oceanologia 64(3), 503–513. https://doi.org/10.1016/j.oceano.2022.03.006

Ghaderi, D., Rahbani, M., 2021. *Tracing suspended matter in Tiab estuary applying ANN and Remote sensing*. Reg. Stud. Mar. Sci. 44, 101788. https://doi.org/10.1016/j.rsma.2021.101788

Ghaderi, D., Rahbani, M., 2020a. *Detecting shoreline change employing remote sensing images (Case study: Beris Port – east of Chabahar, Iran)*. Int. J. Coast. Offshore Eng. 3, 1–8. https://doi.org/10.29252/ijcoe.3.4.1

Ghaderi, D., Rahbani, M., 2020b. *Shoreline change analysis along the coast of Bandar Abbas city, Iran using remote sensing images*. Int. J. Coast. Offshore Environ. Eng. 4, 51–64. https://doi.org/10.22034/ijcoe.2020.149346

Ghanavati, E., Shah-Hosseini, M., Marriner, N., 2021. *Analysis of the Makran Coastline of Iran's Vulnerability to Global Sea-Level Rise*. J. Mar. Sci. Eng. 9, 891. https://doi.org/10.3390/jmse9080891

Godwyn-Paulson, P., Jonathan, M.P., Roy, P.D., Rodríguez-Espinosa, P.F., Muthusankar, G., Muñoz-Sevilla, N.P., Lakshumanan, C., 2021. *Evolution of southern Mexican Pacific coastline: Responses to meteo-oceanographic*

and physiographic conditions. Reg. Stud. Mar. Sci. 47, 101914.
https://doi.org/10.1016/j.rsma.2021.101914

Gunasinghe, G.P., Ruhunage, L., Ratnayake, N.P., Ratnayake, A.S., Samaradivakara, G.V.I., Jayaratne, R., 2021. *Influence of manmade effects on geomorphology, bathymetry and coastal dynamics in a monsoon-affected river outlet in Southwest coast of Sri Lanka*. Environ. Earth Sci. 80, 238.
https://doi.org/10.1007/s12665-021-09555-0

Haghani, S., Leroy, S.A.G., Wesselingh, F.P., Rose, N.L., 2016. *Rapid evolution of coastal lagoons in response to human interference under rapid sea level change: A south Caspian Sea case study*. Quat. Int. 408, 93–112.
https://doi.org/10.1016/j.quaint.2015.12.005

Himmelstoss, E.A., Henderson, R.E., Kratzmann, M.G., Farris, A.S., 2018. *Digital shoreline analysis system (DSAS) version 5.0 user guide*.
https://doi.org/https://doi.org/10.3133/ofr20181179

Hossen, M.F., Sultana, N., 2023. *Shoreline change detection using DSAS technique: Case of Saint Martin Island, Bangladesh*. Remote Sens. Appl. Soc. Environ. 30, 100943.
https://doi.org/10.1016/j.rsase.2023.100943

Hsu, T.-W., Lin, T.-Y., Tseng, I.-F., 2007. *Human Impact on Coastal Erosion in Taiwan*. J. Coast. Res. 234, 961–973.
https://doi.org/10.2112/04-0353R.1

Isaie Moghaddam, E., Allahdadi, M.N., Ashrafi, A., Chaichitehrani, N., 2021. *Coastal system evolution along the southeastern Caspian Sea coast using satellite image analysis: response to the sea level fall during 1994–2015*. Arab. J. Geosci. 14, 771.
https://doi.org/10.1007/s12517-021-07106-2

Johnston, W.G., Cooper, J.A.G., Olynik, J., 2023. *Shoreline change on a tropical island beach, Seven Mile Beach, Grand Cayman: The influence of beachrock and shore protection structures*. Mar. Geol. 457, 107006.
https://doi.org/10.1016/j.margeo.2023.107006

Jumb, V., Sohani, M., Shrivas, A., 2014. *Color Image Segmentation Using K-Means Clustering and Otsu's Adaptive Thresholding*.

Kakroodi, A.A., Kroonenberg, S.B., Goorabi, A., Yamani, M., 2014. *Shoreline Response to Rapid 20th Century Sea-Level Change along the Iranian Caspian Coast*. J. Coast. Res. 298, 1243–1250.
https://doi.org/10.2112/JCOASTRES-D-12-00173.1

Khakhim, N., Kurniawan, A., Pranowo, W.S., Khasanah, E.U., Halilintar, P., 2024. *Shoreline morphological change prognostic model based on spatiotemporal framework imagery data on the northern coast of Java, Indonesia*. Kuwait J. Sci. 51, 100274.
https://doi.org/10.1016/j.kjs.2024.100274

Lahijani, H., Azizpour, J., Arpe, K., Abtahi, B., Rahnama, R., Ghafarian, P., Hamzeh, M.A., Hamzehpour, A., Penchah, M.M., Mahmoudof, S.M., 2023a. *Tracking of sea level impact on Caspian Ramsar sites and potential restoration of the Gorgan Bay on the southeast Caspian coast*. Sci. Total Environ. 857, 158833.
https://doi.org/10.1016/j.scitotenv.2022.158833

Lahijani, H., Leroy, S.A.G., Arpe, K., Crétaux, J.-F., 2023b. *Caspian Sea level changes during instrumental period, its impact and forecast: A review*. Earth-Science Rev. 241, 104428.
https://doi.org/10.1016/j.earscirev.2023.104428

Leroy, S.A.G., Gracheva, R., Medvedev, A., 2022. *Natural hazards and disasters around the Caspian Sea*. Nat. Hazards 114, 2435–2478.
https://doi.org/10.1007/s11069-022-05522-5

Li, Y., Wu, H., 2012. *A Clustering Method Based on K-Means Algorithm*. Phys. Procedia.
https://doi.org/10.1016/j.phpro.2012.03.206

Mageswaran, T., Sachithanandam, V., Sridhar, R., Mahapatra, M., Purvaja, R., Ramesh, R., 2021. *Impact of sea level rise and shoreline changes in the tropical island ecosystem of Andaman and Nicobar region, India*. Nat. Hazards 109, 1717–1741.
https://doi.org/10.1007/s11069-021-04895-3

Mariotti, G., Hein, C.J., 2022. *Lag in response of coastal barrier-island retreat to sea-level rise*. Nat. Geosci. 15, 633–638.
https://doi.org/10.1038/s41561-022-00980-9

McFEETERS, S.K., 1996. *The use of the Normalized Difference Water Index (NDWI) in the delineation of open water features*. Int. J. Remote Sens. 17, 1425–1432.
https://doi.org/10.1080/01431169608948714

Medvedev, I.P., Kulikov, E.A., Fine, I. V., 2020. *Numerical modelling of the Caspian Sea tides*. Ocean Sci. 16, 209–219.
https://doi.org/10.5194/os-16-209-2020

Medvedev, I.P., Kulikov, E.A., Rabinovich, A.B., 2017. *Tidal oscillations in the Caspian Sea*. Oceanology 57(3), 360–375.
https://doi.org/10.1134/S0001437017020138

Mishra, M., Guria, R., Paul, S., Baraj, B., Santos, C.A.G., dos Santos, C.A.C., Silva, R.M. da, 2024. *Geo-ecological, shoreline dynamic, and flooding impacts of Cyclonic Storm Mocha: A geospatial analysis*. Sci. Total Environ. 917, 170230.
https://doi.org/10.1016/j.scitotenv.2024.170230

Murray, J., Adam, E., Woodborne, S., Miller, D., Xulu, S., Evans, M., 2023. *Monitoring Shoreline Changes along the Southwestern Coast of South Africa from 1937 to 2020 Using Varied Remote Sensing Data and Approaches*. Remote Sens. 15, 317.
https://doi.org/10.3390/rs15020317

Nassar, K., Mahmod, W.E., Fath, H., Masria, A., Nadaoka, K., Negm, A., 2019. *Shoreline change detection using DSAS technique: Case of North Sinai coast, Egypt*. Mar. Geores. Geotechnol. 37, 81–95.
https://doi.org/10.1080/1064119X.2018.1448912

NAVIONICS, 2023. *Navionics ChartViewer*. https://webapp.navionics.com/?lang=en#boating (accessed 3.25.24).

Nijamir, K., Ameer, F., Thennakoon, S., Herath, J., Iyoob, A.L., Zahir, I.L.M., Sabaratnam, S., Fathima Jisna, M.V., Madurapperuma, B., 2023. *Geoinformatics application for estimating and forecasting of periodic shoreline changes in the east coast of Ampara District, Sri Lanka*. Ocean Coast. Manag. 232, 106425. https://doi.org/10.1016/j.ocecoaman.2022.106425

Parthasarathy, K.S.S., Deka, P.C., 2019. *Remote sensing and GIS application in assessment of coastal vulnerability and shoreline changes: a review*. ISH J. Hydraul. Eng. 27, 1–13. https://doi.org/10.1080/09715010.2019.1603086

Pereira-Sandoval, M., Ruescas, A., Urrego, P., Ruiz-Verdú, A., Delegido, J., Tenjo, C., Soria-Perpinyà, X., Vicente, E., Soria, J., Moreno, J., 2019. *Evaluation of Atmospheric Correction Algorithms over Spanish Inland Waters for Sentinel-2 Multi Spectral Imagery Data*. Remote Sens. 11, 1469. https://doi.org/10.3390/rs11121469

Pisanti, A., Magrì, S., Ferrando, I., Federici, B., 2022. *Sea water turbidity analysis from sentinel-2 images: atmospheric correction and bands correlation*. Int. Arch. Photogramm. Remote Sens. Spat. Inf. Sci. XLVIII-4/W, 371–378. https://doi.org/10.5194/isprs-archives-XLVIII-4-W1-2022-371-2022

Prange, M., Wilke, T., Wesselingh, F.P., 2020. *The other side of sea level change. Commun*. Earth Environ. 1, 69. https://doi.org/10.1038/s43247-020-00075-6

Rahbani, M., Ghaderi, D., 2024. *Long term investigation on shoreline changes of an Island, inside a Gulf (Hormuz Island)*. Reg. Stud. Mar. Sci. 71, 103399. https://doi.org/10.1016/j.rsma.2024.103399

Rahbani, M., Ghaderi, D., Shamsaie, R., Salari, Z., Permas, A., 2023a. *Investigation on the seasonal transformation of Tiab estuary's shoreline using RS and GIS techniques*. Int. J. Coast. Offshore Environ. Eng. 8, 56–64. https://doi.org/10.22034/ijcoe.2023.395872.1029

Rahbani, M., Ghaderi, D., Shamsaie, R., Zarafshan, S., Razi, A., 2023b. *Investigating the impact of earthquakes on man-made structures in the vicinity of coastlines (Case study, earthquake on 2nd of July 2022, Sayekhosh)*. J. Earth Sp. Phys. https://doi.org/10.22059/jesphys.2023.353910.1007494

Rajasree, B.R., Deo, M.C., Sheela Nair, L., 2016. *Effect of climate change on shoreline shifts at a straight and continuous coast*. Estuar. Coast. Shelf Sci. 183, 221–234. https://doi.org/10.1016/j.ecss.2016.10.034

Rashmi, C., Chaluvaiah, S., Kumar, G.H., 2016. *An Efficient Parallel Block Processing Approach for K -Means Algorithm for High Resolution Orthoimagery Satellite Images*. Procedia Comput. Sci. https://doi.org/10.1016/j.procs.2016.06.0252

Renssen, H., Lougheed, B.C., Aerts, J.C.J.H., de Moel, H., Ward, P.J., Kwadijk, J.C.J., 2007. *Simulating long-term Caspian Sea level changes: The impact of Holocene and future climate conditions*. Earth Planet. Sci. Lett. 261, 685–693. https://doi.org/10.1016/j.epsl.2007.07.0372

Rezaee, S.M., Golshani, A., Abedi, S., 2022. *Shoreline changes at Fereydounkenar Port in light of Caspian Sea's water level fluctuations*. Reg. Stud. Mar. Sci. 53, 102393. https://doi.org/10.1016/j.rsma.2022.1023932

Roshan, G., Moghbel, M., Grab, S., 2012. *Modeling Caspian Sea water level oscillations under different scenarios of increasing atmospheric carbon dioxide concentrations*. Iranian J. Environ. Health Sci. Eng. 9, 24. https://doi.org/10.1186/1735-2746-9-242

Samant, R., Prange, M., 2023. *Climate-driven 21st century Caspian Sea level decline estimated from CMIP6 projections*. Commun. Earth Environ. 4, 357. https://doi.org/10.1038/s43247-023-01017-82

Santos, C.A.G., do Nascimento, G.R., Freitas, L.M.T., Batista, L.V., Zerouali, B., Mishra, M., Silva, R.M. da, 2024. *Coastal evolution and future projections in Conde County, Brazil: A multi-decadal assessment via remote sensing and sea-level rise scenarios*. Sci. Total Environ. 915, 169829. https://doi.org/10.1016/j.scitotenv.2023.1698292

Santos, C.A.G., Nascimento, T.V.M. do, Mishra, M., Silva, R.M. da, 2021. *Analysis of long- and short-term shoreline change dynamics: A study case of João Pessoa city in Brazil*. Sci. Total Environ. 769, 144889. https://doi.org/10.1016/j.scitotenv.2020.1448892

Seenath, A., 2022. *On simulating shoreline evolution using a hybrid 2D/one-line model*. Coast. Eng. 178, 104216. https://doi.org/10.1016/j.coastaleng.2022.1042162

Shamsaie, R., Ghaderi, D., 2025. *Comparison of efficiency of spectral (NDWI) and SAR (GRD) method in shoreline detection: A novel method of integrating GRD and SLC products of sentinel-1 satellite*. Reg. Stud. Mar. Sci. 84, 104132. https://doi.org/10.1016/j.rsma.2025.104132

Shirazi, A.S., Qashqaei, A.T., Faezi, S., Khaleghi, S., Moghaddamipour, N., Ebrahimi, T., Hassan, S.K., Chilvers, B.L., 2023. *First confirmed records of white-coat pups of the Endangered Caspian seal Pusa caspica on the coast of Iran*. Oryx 57, 784–787. https://doi.org/10.1017/S003060532200148X

Soriano-González, J., Urrego, E.P., Sòria-Perpinyà, X., Angelats, E., Alcaraz, C., Delegido, J., Ruíz-Verdú, A., Tenjo, C., Vicente, E., Moreno, J., 2022. *Towards the Combination of C2RCC Processors for Improving Water Quality Retrieval in Inland and Coastal Areas*. Remote Sens. 14, 1124. https://doi.org/10.3390/rs14051124

Thieler, E.R., Himmelstoss, E.A., Zichichi, J.L., Ergul, A., 2009. *The Digital Shoreline Analysis System (DSAS) version 4.0-an ArcGIS extension for calculating shoreline change*. https://doi.org/10.3133/ofr20081278

Toorani, M., Kakroodi, A.A., Yamani, M., Naderi Beni, A., 2021. *Monitoring shoreline shift under rapid sea-level change on the Caspian Sea observed over 60 years of satellite and aerial photo records*. J. Great Lakes Res. 47, 812–828. https://doi.org/10.1016/j.jglr.2021.02.006

Toure, S., Diop, O., Kpalma, K., Maiga, A., 2019. *Shoreline Detection using Optical Remote Sensing: A Review*. ISPRS Int. J. Geo-Information 8, 75. https://doi.org/10.3390/ijgi8020075

Vallarino Castillo, R., Negro Valdecantos, V., Moreno Blasco, L., 2022. *Shoreline Change Analysis Using Historical Multispectral Landsat Images of the Pacific Coast of Panama*. J. Mar. Sci. Eng. 10, 1801. https://doi.org/10.3390/jmse10121801

Weerasingha, W.A.D.B., Ratnayake, A.S., 2022. *Coastal landform changes on the east coast of Sri Lanka using remote sensing and geographic information system (GIS) techniques*. Remote Sens. Appl. Soc. Environ. 26, 100763. https://doi.org/10.1016/j.rsase.2022.100763

Yan, D., Yao, X., Li, J., Qi, L., Luan, Z., 2021. *Shoreline Change Detection and Forecast along the Yancheng Coast Using a Digital Shoreline Analysis System*. Wetlands 41, 47. https://doi.org/10.1007/s13157-021-01444-3

Yum, S.-G., Park, S., Lee, J.-J., Adhikari, M. Das, 2023. *A quantitative analysis of multi-decadal shoreline changes along the East Coast of South Korea*. Sci. Total Environ. 876, 162756. https://doi.org/10.1016/j.scitotenv.2023.162756

Zambrano-Medina, Y.G., Plata-Rocha, W., Monjardin-Armenta, S.A., Franco-Ochoa, C., 2023. *Assessment and Forecast of Shoreline Change Using Geo-Spatial Techniques in the Gulf of California*. Land 12, 782. https://doi.org/10.3390/land12040782

Zanganeh, M., Chaji, A., 2024. *A new aspect of the ApEn application to improve the PSO-ANFIS model to forecast Caspian Sea levels*. Reg. Stud. Mar. Sci. 69, 103347. https://doi.org/10.1016/j.rsma.2023.103347